Quantum spin fluctuations and hydrogen bond network in the antiferromagnetic natural mineral henmilite

Hajime Yamamoto,[1] Terutoshi Sakakura,[1] Harald O. Jeschke,[2] Noriyuki Kabeya,[3] Kanata Hayashi,[4] Yuya Ishikawa,[4] Yutaka Fujii,[4] Shunji Kishimoto,[5] Hajime Sagayama,[5] Kei Shigematsu,[6,7] Masaki Azuma,[6,7] Akira Ochiai,[3] Yukio Noda,[1] and Hiroyuki Kimura[1]

[1]*Institute of Multidisciplinary Research for Advanced Materials, Tohoku University, Katahira 2-1-1, Aoba, Sendai 980-8577, Japan*
[2]*Research Institute for Interdisciplinary Science, Okayama University, Okayama 700-8530, Japan*
[3]*Department of Physics, Tohoku University, Aoba 6-3, Aoba, Sendai 980-8577, Japan*
[4]*Research Center for Development of Far-Infrared Region, University of Fukui, Bunkyo 3-9-1, Fukui 910-8507, Japan*
[5]*Photon Factory and Condensed Matter Research Center, Institute of Materials Structure Science, High Energy Accelerator Research Organization, Oho 1-1, Tsukuba 305-0801, Japan*
[6]*Laboratory for Materials and Structures, Tokyo Institute of Technology, Nagatsuta 4259, Midori, Yokohama 226-8503, Japan*
[7]*Kanagawa Institute of Industrial Science and Technology (KISTEC), Ebina 243-0435, Japan*

(Received 25 May 2021; accepted 27 September 2021; published 13 October 2021)

Henmilite $\{Ca_2Cu(OH)_4[B(OH)_4]_2\}$ is a blue calcium copper borate mineral found only in the Fuka mine, Okayama Prefecture, Japan. Crystal structure refinement, magnetic and specific heat measurements, and density functional theory (DFT) calculations are performed to clarify its magnetic properties. Synchrotron x-ray diffraction experiments reveal that the hydrogen-bonded chains are arranged in an antiferroelectric manner, doubling the unit cell along the *a* axis. An antiferromagnetic transition is observed at 0.2 K at zero magnetic field. Furthermore, a dome-shaped antiferromagnetic ordering region exists in the temperature–magnetic-field phase diagram, indicating the presence of quantum spin fluctuations. The obtained crystal structure in combination with DFT calculations suggests that the system has a coupled two-leg ladder magnetic lattice, explaining the very low ordering temperature.

DOI: 10.1103/PhysRevMaterials.5.104405

I. INTRODUCTION

Spin-1/2 low-dimensional antiferromagnets have been widely studied because of their potential to exhibit fascinating properties such as quantum spin liquid phases [1], Bose-Einstein condensation of magnons [2], or a quantum spin-nematic phase [3]. One-dimensional systems such as spin chains [4] or spin ladders [5] are famous for their unusual behavior. Quantum fluctuations in magnetic materials are strong in systems containing spin-1/2 magnetic ions such as Ti^{3+} [6] or V^{4+} [7]. However, a particularly large number of inorganic $S = 1/2$ materials are realized with Cu^{2+} ions [8]. Natural minerals containing Cu^{2+} have been of much interest due to the diversity of their crystal structures [9]. For example, herbertsmithite, $ZnCu_3(OH)_6Cl_2$ [10], and variants of barlowite, $Cu_4BrF(OH)_6$ [11], are known as candidate materials for quantum spin liquids, and azurite, $Cu_3(CO_3)_2(OH)_2$ [12,13], is known as a one-dimensional diamond chain system. Very recently, the mineral atlasovite, $KCu_6FeBiO_4(SO_4)_5Cl_2$, has inspired the synthesis of the square-kagome-lattice material $KCu_6AlBiO_4(SO_4)_5Cl$ [14]. Investigating copper minerals promises further surprises and the discovery of new physical phenomena. The natural mineral henmilite, $Ca_2Cu(OH)_4[B(OH)_4]_2$, is a calcium hydroxy borate mineral (Fig. 1) found only in the Fuka mine, Okayama Prefecture, Japan. Fuka is a limestone quarry, and its metamorphic aureole is famous for a peculiar occurrence of high-temperature skarn. These minerals resulted from the intrusion of quartz monzonite into marine carbonate rocks. Henmilite was first reported in 1986 [15,16].

According to previous reports [16], the crystal structure is triclinic with a space group of $P\bar{1}$, and the lattice parameters are $a = 5.7617(5)$ Å, $b = 7.9774(6)$ Å, $c = 5.6488(4)$ Å, $\alpha = 109.611(6)^\circ$, $\beta = 91.473(1)^\circ$, and $\gamma = 83.686(7)^\circ$. Square planar $Cu(OH)_4$ units are connected via a complex hydrogen bond network in the crystal structure, resulting in a spin-1/2 distorted square (rectangular) lattice. It was challenging to detect the correct hydrogen positions with the accuracy of the single-crystal x-ray diffraction analysis methodology. In the reported crystal structure [16], the occurrence of two hydrogen atoms on a single hydrogen bond suggests that this might be an average structure and the reality is more complex. The determination of the precise crystal structure is crucial for the investigation of complex magnetism because the calculated Hamiltonian parameters can be extremely sensitive to structural details; an example is the well-known triangular lattice material Cs_2CuCl_4 [17]. This is also true for hydrogen positions [18]; for clinoclase, $Cu_3(AsO_4)(OH)_3$ [19], it has been argued that the position of the hydrogen is not a negligible factor in determining the magnetic properties. In the case of kapellasite, $ZnCu_3(OH)_6Cl_2$,

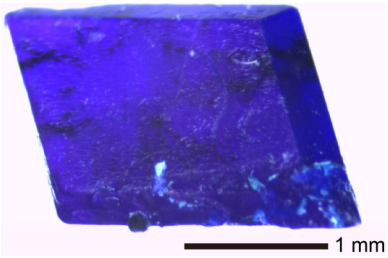

FIG. 1. Image of a henmilite crystal.

the position of hydrogen can even flip the sign of an important exchange coupling [20].

In this paper, we performed a crystal structure refinement, magnetic and specific heat measurements, and electronic structure calculations of henmilite. Hydrogen-bonded chains are arranged in an antiferroelectric manner, doubling the unit cell along the a-axis (Fig. 2). The obtained structure combined with the calculations reveals that the system is a coupled two-leg spin ladder, which is regarded as a spin-gapped system [21–24]. An antiferromagnetic transition was observed at an extremely low temperature of 0.2 K at 0 T and 0.8 K at 3 T ($\mu_0 H \parallel b^*$). Furthermore, an anomalous dome-shaped antiferromagnetic ordering region was observed in the temperature–magnetic-field phase diagram. This behavior can be linked to effects of quantum fluctuations associated with the geometry of the magnetic lattice.

II. EXPERIMENTAL AND COMPUTATIONAL DETAILS

A. Crystal structure refinement

The samples of henmilite were purchased from a mineral store. The single crystals were picked mechanically from parent rocks. These single crystals were washed with a dilute hydrochloric acid solution (∼2 wt %) to remove amorphous impurities on the surface. The sample phase purity was determined using powder x-ray diffraction (XRD) and superconducting quantum interference device (SQUID) measurements. The chemical composition was determined using an electron probe microanalyzer [wavelength-dispersive spectrometer (WDS), JXA-8200; JEOL]. For synchrotron XRD (SXRD) analysis, the single crystal was shaped into a sphere using a spheronizer. The space group and unit cell were determined using an area detector at BL-8B, Photon Factory, High Energy Accelerator Research Organization (KEK), Tsukuba, Japan. For the space group determination, a monochromatic beam $\lambda = 0.995\,953$ Å was used. A four-circle diffractometer at BL-14A, Photon Factory [25], was used to collect data for refining the lattice and structural parameters. The multiple-diffraction-avoidance technique was applied to reduce the systematic error [26]. A customized avalanche photodiode detector was used for reducing statistical error due to counting statistics [27,28]. The synchrotron x-ray wavelength was $\lambda = 0.684\,31(2)$ Å. A spherical single crystal of henmilite with 140-μm diameter was used as the specimen. The crystallographic software JANA 2006 was used for the refinement. Refined parameters are summarized in Table S1 of the Supplemental Material [29]. All structure drawings are done with VESTA [30].

B. Physical property measurements: Magnetic and specific heat measurements

The temperature dependence of the magnetic susceptibility of the powder sample ($\mu_0 H = 0.1$ T, 2–300 K) and the single crystal along the a^*, b^*, and c^* directions ($\mu_0 H = 0.1$ T, 2–30 K) and the magnetic field dependence of the magnetization ($T = 2$ K, up to 5 T) were measured using a SQUID magnetometer (MPMS-XL; Quantum Design). Additionally, specific heat measurements along the b^* direction were performed using the quasiadiabatic method (handmade calorimeter) between 0.1 K and either 4 or 10 K with fields up to 15 T.

C. Computational methods

We perform all electron density functional theory calculations using the full-potential local-orbital (FPLO) code [31]. We use the generalized gradient approximation (GGA) exchange-correlation functional [32]. Furthermore, we deal with the strong electronic correlations in the Cu^{2+} $3d$ orbitals with a GGA+U correction [33]. While the Hund's rule coupling J_H is kept fixed at $J_H = 1$ eV in accordance with earlier studies [34,35], we vary the on-site Coulomb

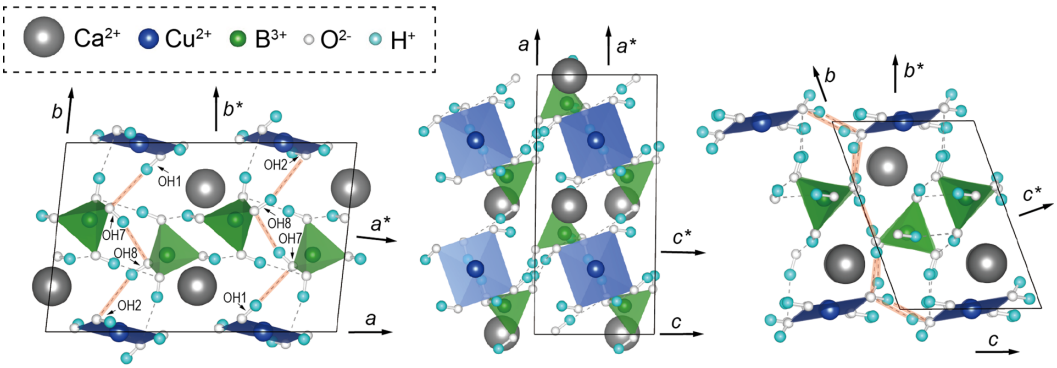

FIG. 2. Crystal structure of henmilite $Ca_2Cu(OH)_4[B(OH)_4]_2$ in projection along [001] (left), [010] (center), and [100] (right). Hydrogen bonds highlighted with red lines show the antiferroelectric chains.

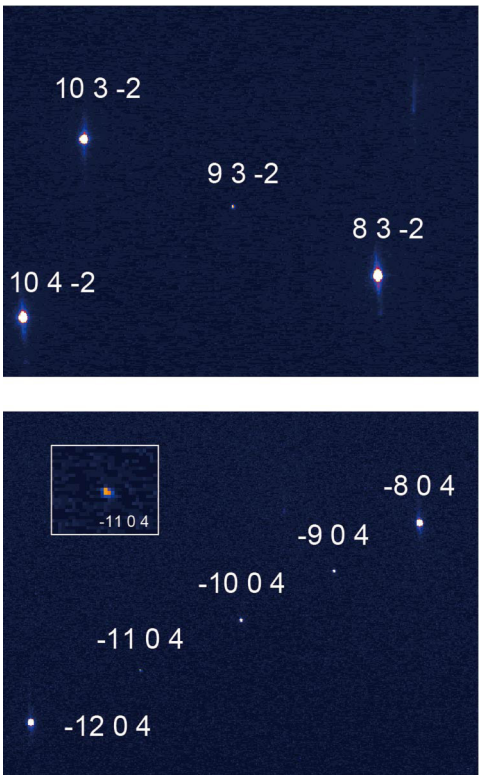

FIG. 3. Diffraction spots of a henmilite single crystal. Odd h index reflections correspond to superlattice reflections $(h/2\,k\,l)$ with the notation of the previously reported setting [15,16]. The inset shows a magnified view of the $(-11\,0\,4)$ reflection.

interaction U. For the GGA+U calculations, an atomic limit double-counting correction was used.

III. RESULTS AND DISCUSSION

A. Crystal structure and hydrogen bond network

Superlattice reflections, which correspond to $(1/2h\,k\,l)$ with the same notation as in the previous setting [15,16], were detected in the SXRD data (Fig. 3). These reflections were not reported in previous studies. The correct lattice parameters of henmilite were determined, which turn out to be doubled along the a axis. {The parameters are summarized in the Supplemental Material [29] and crystallographic information file (CIF)}. In our structure refinement, all hydrogen positions were successfully determined, as shown in Fig. 2. As seen in the figure, hydrogens make a complex hydrogen bond network. The superlattice structure originates from the hydrogen bond network and antiferrodistortive displacement of each atom, for example, an alternate displacement of Cu along the a axis. The chains comprising O1-H1 (OH1), O2-H2 (OH2), O7-H7 (OH7), and O8-H8 (OH8) are arranged in an antiferroelectric manner along the a axis, namely, hydrogen-bond-type antiferroelectrics. Their local electric dipoles roughly orient parallel to the b axis (b* direction), as shown in Fig. 2. The hydrogen bond lengths are summarized in Table S2 of the Supplemental Material [29]. The hydrogen electron cloud is drawn toward the oxygen due to covalency. Thus the O-H bond lengths of 0.7–0.8 Å

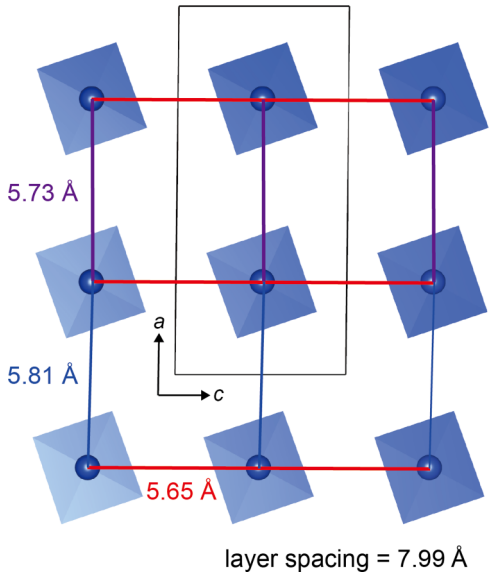

FIG. 4. The Cu sublattice and the Cu-Cu bond lengths.

are shorter than the typical lengths obtained from neutron data, e.g., 1.0 Å for 5-bromo-9-hydroxyphenalenon [36,37]. The superlattice structure changes the aspect of the expected nature of the magnetic spin system. The Cu-Cu bond lengths are 5.65, 5.73, and 5.81 Å, indicating that the system could be regarded as intermediate between a square (rectangular) lattice and a two-leg ladder lattice (Fig. 4).

B. Magnetic properties

Figures 5 and 6 exhibit the temperature dependence of the magnetic susceptibility of the powder and the single crystal in the a^*, b^*, and c^* directions, respectively. The Curie-Weiss fit presented in Fig. 5 demonstrates the spin-1/2 antiferromagnetic nature. A broad peak was observed around 3 K, indicating the low-dimensional nature, as shown in Fig. 6. The behavior was reproduced by a spin-1/2 square-lattice model

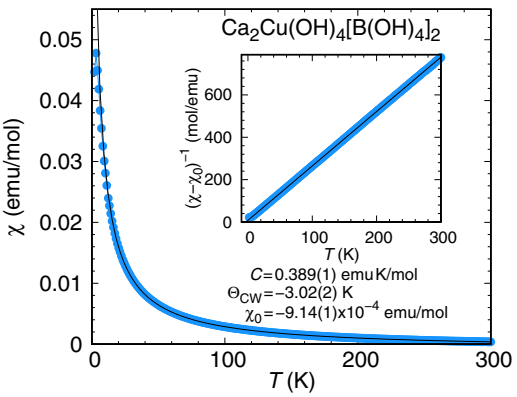

FIG. 5. Temperature dependence of magnetic susceptibility χ of a henmilite powder sample (the zero-field process, solid blue circles), with Curie-Weiss fit $\chi = \frac{C}{T-\Theta_{CW}} + \chi_0$ (black curve), where C is the Curie constant, Θ_{CW} is the Weiss temperature, and χ_0 is a diamagnetic part. The fitting was performed between 30 and 300 K. Inset: Inverse of χ after substraction of χ_0.

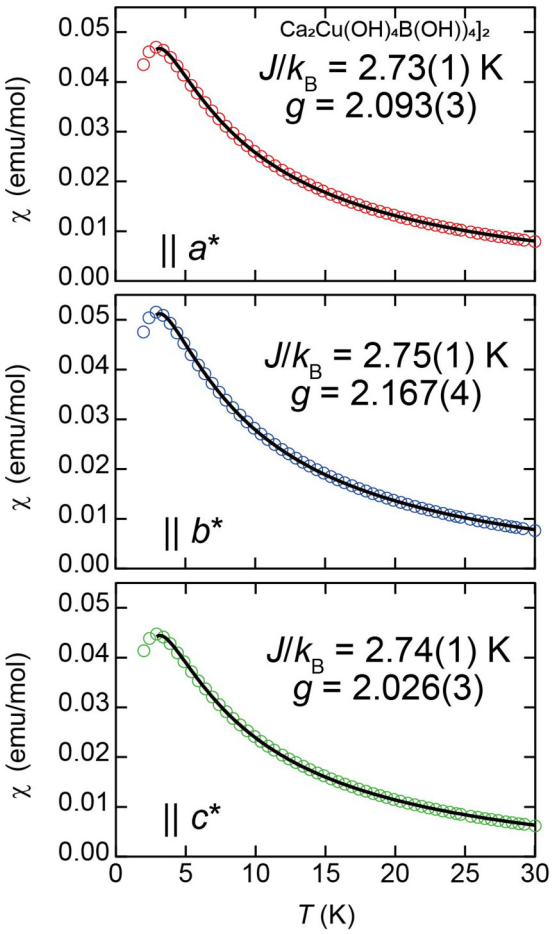

FIG. 6. Temperature dependence of magnetic susceptibility of a henmilite single crystal in the a^* (red), b^* (blue), and c^* (green) directions. Black curves represent the fitting result for the field cooling process. The applied magnetic field was 0.1 T.

with a temperature-independent term:

$$\chi(T) = \frac{Ng^2\mu_B^2}{4k_BT}\left[1 + \left(\frac{J}{k_BT}\right) + \frac{1}{2}\left(\frac{J}{k_BT}\right)^2 + \frac{1}{6}\left(\frac{J}{k_BT}\right)^3 + \frac{1}{64}\left(\frac{J}{k_BT}\right)^4\right]^{-1} + \chi_0, \quad (1)$$

where N is the Avogadro constant, g is the gyromagnetic ratio, J is the nearest-neighbor exchange, and k_B is the Boltzmann constant [38,39]. An antiferromagnetic exchange of $J \sim 2.7$ K was obtained. The g factor in the b^* direction is slightly larger than those along the other directions, which should be caused by the spin-orbital coupling of the Cu^{2+} ion in the square planar coordination. Figure 7 displays the magnetic field dependence of magnetization at 2 K (M-H curve) of randomly oriented henmilite crystals (powder). A slight inflection point was observed around 3 T. This nonlinearity in the magnetization curve vanishes completely at 4 K (Fig. S3 of the Supplemental Material).

Specific heat measurements at a temperature as low as 0.1 K and magnetic fields up to 15 T were performed to clarify the presence of a magnetic transition. The results are shown in Fig. 8(a). The nuclear specific heats were subtracted from

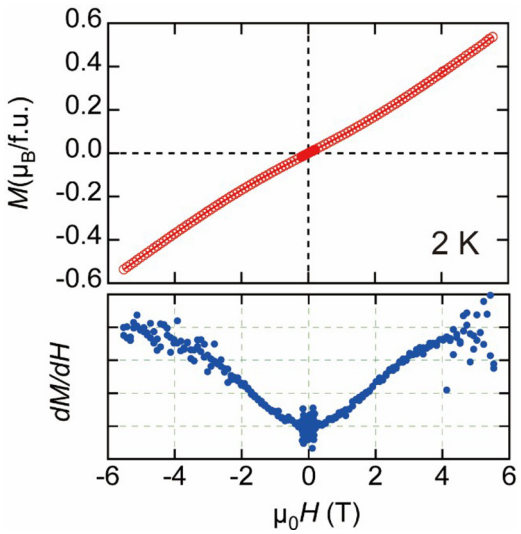

FIG. 7. Magnetic field dependence of magnetization (M-H curve) of randomly oriented henmilite crystals (powder).

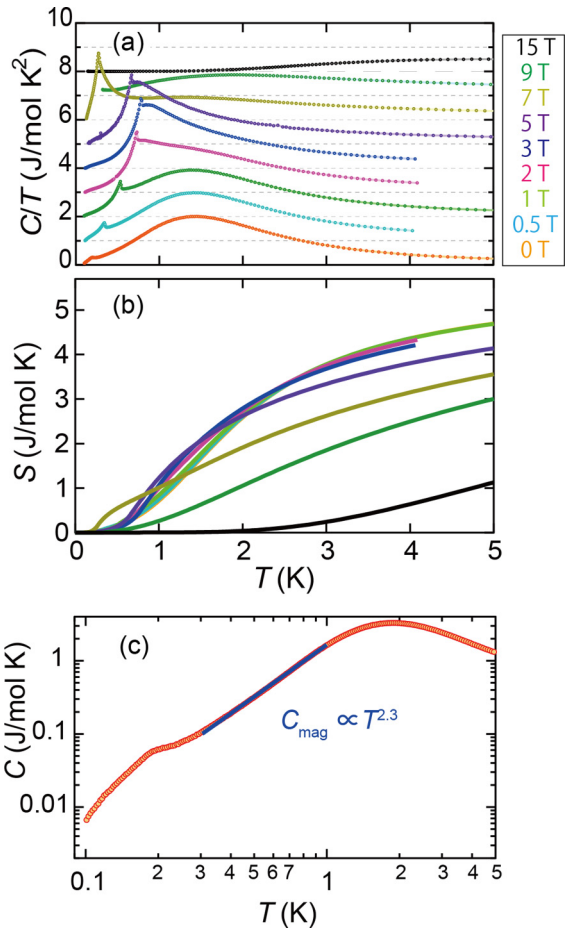

FIG. 8. (a) Temperature dependence of specific heat in magnetic fields up to 15 T ($\mu_0 H \parallel b^*$). All data are offset by 1 J/mol K^2. (b) Entropy change estimated from the specific heat results. (c) Temperature dependence of specific heat (logarithmic) at 0 T and the fitting of $C = AT^\alpha$ between 0.4 and 1 K, where A is a constant, T is the temperature, and α is the exponent.

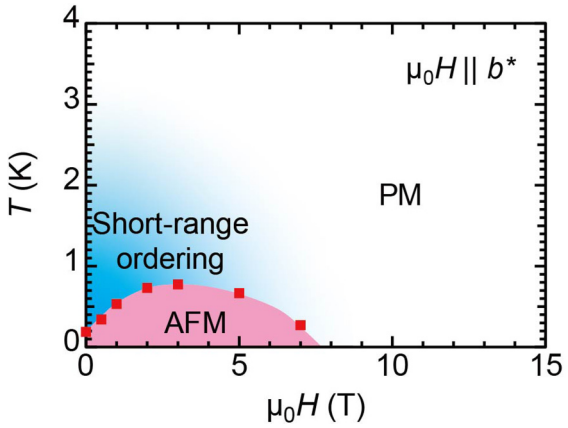

FIG. 9. The magnetic phase diagram of henmilite ($\mu_0 H \parallel b^*$) in the magnetic-field–temperature plane (zero-field cooling process). AFM and PM, antiferromagnetic and paramagnetic regions, respectively.

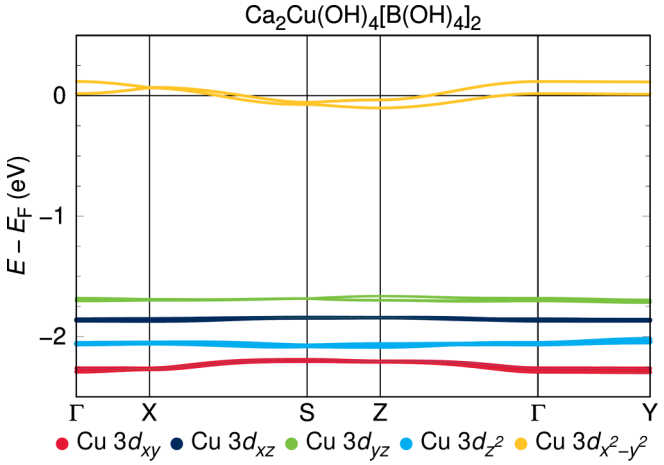

FIG. 10. Band structure of $Ca_2Cu(OH)_4[B(OH)_4]_2$ obtained from GGA calculations. Orbital weights for Cu $3d$ orbitals are highlighted.

the data, as described in the Supplemental Material. A λ-like peak at 0.2 K and a broad peak at <3 K were observed at 0 T. The magnetic entropy change at 0 T and <5 K is ∼5 J mol^{-1} K^{-1} [Fig. 8(b)], nearly consistent with the theoretical value expected for a spin-1/2 system, $R\ln(2S+1) = 5.75$ J mol^{-1} K^{-1}. The specific heat exhibited a power-law behavior of $C \propto T^{\sim 2.3}$, which indicated the two-dimensional nature of this spin system [Fig. 8(c)] [40]. We have concluded that the λ-like peak and the broad peak correspond to an antiferromagnetic transition and the development of short-range ordering, respectively. The anomaly in the M-H curve should be attributed to the suppression of the short-range ordering. The antiferromagnetic transition temperature increased with increasing applied magnetic field up to 3 T along the b^* direction, while the transition temperature decreased gradually at higher magnetic fields. The transition was no longer observed above 9 T. Figure 9 shows the magnetic phase diagram established in the temperature–magnetic-field plane based on the results. A dome-shaped antiferromagnetic region appears in the diagram. Such behavior does not coincide with that of common antiferromagnets [41], where the transition temperature decreases with increasing magnetic field. Interestingly, such dome-shaped ordered phases have been observed in some spin-1/2 low-dimensional antiferromagnets [42–44]. The next section will be devoted to the microscopic Hamiltonian governing henmilite.

C. Origin of quantum fluctuations

The band structure of $Ca_2Cu(OH)_4[B(OH)_4]_2$ is shown in Fig. 10; there are ten bands with dominant Cu $3d$ character from the two Cu^{2+} ions in the unit cell. Crossing the Fermi level, there are only the two bands of Cu $3d_{x^2-y^2}$ character. The band at the Fermi level is narrow, signifying only small Cu-Cu hopping and consequently small Cu-Cu exchange. Dispersions along k_x and k_z are comparable, while dispersion along k_y is negligible. This indicates that at least electronically, the material is two dimensional. The GGA band structure with bands crossing the Fermi level is shown here because it characterizes the chemical properties of the material. For the exchange interactions, the GGA+U functional at the relevant value of $U = 7.7$ eV [see Fig. 11(a) for the choice of U] opens a gap of $E_g = 3.6$ eV for all spin configurations.

Next, we determine the Heisenberg Hamiltonian characterizing henmilite using the energy mapping method [45,46]. For this purpose, we create a $2 \times 1 \times 3$ supercell with 12 independent Cu^{2+} sites. This allows us to determine all the nearest and next-nearest in-plane exchange couplings in the distorted square lattice of henmilite; these seven different exchange paths are shown in Fig. 11(b). By performing the energy mapping on the average crystal structure of henmilite [16], we have verified that the material has very two-dimensional exchange, with interlayer exchange couplings below 1% of the dominant couplings. The energy mapping has been performed for six values of the on-site interaction U, as shown in Fig. 11(a). See the Supplemental Material [29] for a table with all the determined couplings. The Curie-Weiss temperature can be determined from the equation

$$\Theta_{\mathrm{CW}} = -\frac{2}{3}S(S+1) \times \left(J_1 + \frac{J_2}{2} + \frac{J_3}{2} + \frac{J_4}{2} + \frac{J_6}{2} + \frac{J_8}{2} + \frac{J_9}{2}\right). \quad (2)$$

We use the experimentally determined Curie-Weiss temperature $\Theta_{\mathrm{CW}} = -3$ K to select the relevant on-site interaction as $U = 7.7$ eV; this yields the set of Heisenberg Hamiltonian parameters $J_1 = 3.59(1)$, $J_2 = 3.48(1)$, $J_3 = 0.89(1)$, $J_4 = 0.14(1)$, $J_6 = 0.00(1)$, $J_8 = 0.20(1)$, and $J_9 = 0.19(1)$ K. Note that the value of the on-site Coulomb repulsion U is close to values around $U = 8$ eV that have been found to describe many magnetic materials based on Cu^{2+} correctly [47,48]. Thus the newly determined, lower-symmetry crystal structure reveals that the magnetism of henmilite is not the two-dimensional one of a rectangular lattice but is in reality of one-dimensional spin ladder type. J_1 and J_2 are of nearly equal strength and form ladders running along the c direction. They are coupled in the ac plane by J_3, which

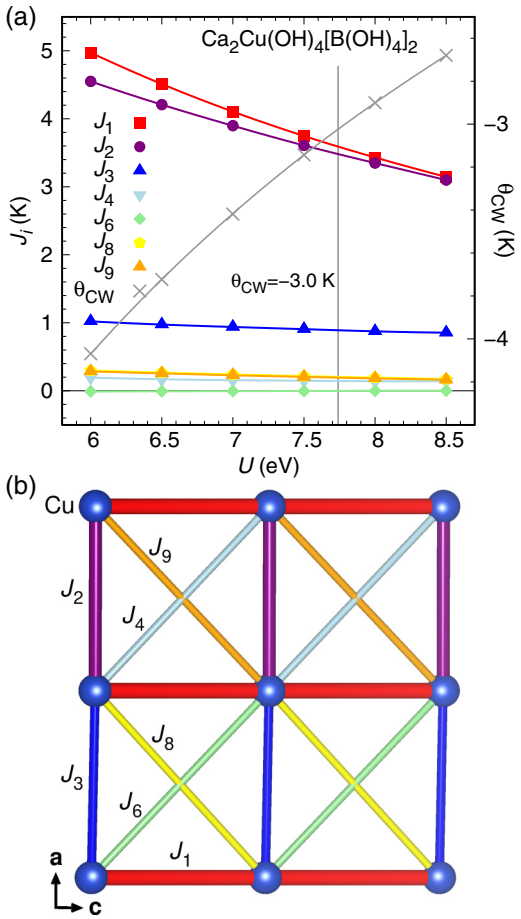

FIG. 11. (a) Exchange interactions of henmilite extracted by DFT energy mapping. Couplings are shown as a function of local Coulomb repulsion U while Hund's rule coupling was fixed to J_H = 1 eV. J_1 and J_2 dominate, making henmilite a two-leg spin ladder compound, with an exchange network as shown in (b).

is only 25% of J_1. Connecting the three largest exchange couplings of henmilite to the new crystal structure, there is J_1, where exchange is along a hydrogen bond while for J_2 and J_3 this is not the case. The Cu-Cu distances of 5.73 Å for J_2 and 5.81 Å for J_3 are very similar. A significant difference, however, is the orientation of the OH groups involved in the exchange paths; as measured by the H-O-O-H dihedral angle, they are nearly coplanar for the J_3 bond, while they are nearly orthogonal for the J_2 bond. This structural distinction between the two exchange paths is most likely responsible for the different magnitudes of J_2 and J_3; as noted above, such sensitivity of magnetic exchange to hydrogen bonds is known [19,20]. Thus the DFT calculations established that henmilite is intermediate between isolated spin ladders and a fully two-dimensional rectangular or square lattice. Furthermore, next-nearest-neighbor couplings $J_4 = 0.04J_1$, $J_8 = 0.06J_1$, and $J_9 = 0.05J_1$ provide small but nonzero frustration effects. Indeed, the Néel temperature is more than ten times lower than the experimental value of J, which is unusual for common square-lattice antiferromagnets [42,49]. A previous theoretical study of the anisotropic dimerized square lattice as defined by J_1, J_2, and J_3 suggests that the ground state of a model with the parameter values of henmilite would be in a spin-gapped dimerized phase but in close proximity to an antiferromagnetic long-range ordered phase [50]. We believe that the low-dimensional pattern defined by the magnetic exchange interactions generates quantum spin fluctuations, which result in the anomalous dome-shaped antiferromagnetic region. The magnetic ordering was subdued down to 0.2 K in zero magnetic field by the quantum spin fluctuations. This effect is suppressed by an external field of up to 3 T, leading to the pronounced increase in the antiferromagnetic transition temperature. The higher magnetic field rather destabilizes the antiferromagnetic ordering. Further studies, such as neutron experiments, are necessary to elucidate details of the spin structure and dynamics.

IV. CONCLUSIONS

In summary, we performed crystal structure refinement, magnetic and specific heat measurements, and DFT calculations to understand the magnetic properties of henmilite. We find that the hydrogen bond network has an important influence on the crystal structure; we obtain a $P\bar{1}$ space group with a unit cell that is doubled compared with the previously published structure [16]. This discovery is crucial for understanding the magnetism of henmilite. Our DFT energy mapping yields a Heisenberg Hamiltonian which translates the small lattice distortion into a substantial magnetic distortion away from the rectangular lattice that can be expected and calculated from the known average crystal structure. Henmilite is described by antiferromagnetic exchange couplings that form weakly coupled two-leg spin ladders. This in turn explains the very low ordering temperature we discover in our magnetic measurements. In an applied magnetic field, this magnetically ordered phase forms an unusual dome shape in the temperature-field phase diagram which we ascribe to the influence of strong quantum fluctuations. Thus we observe in the natural mineral henmilite an essential connection among a crystal structure distortion, dimensionality lowering, and the enhancement of spin fluctuations.

ACKNOWLEDGMENTS

The authors thank Prof. Masakazu Matsubara and Daiki Sekine (Tohoku University), Dr. Takayuki Asano (University of Fukui), Dr. Koji Kaneko (Japan Atomic Energy Agency), and Dr. Koichi Momma (National Museum of Nature and Science) for productive discussions. This work has been financially supported by the TEPCO Memorial Foundation (Grant No. 19-022), Grant-in-Aid for Scientific Research (Grant No. 19K15280) from the Japan Society for the Promotion of Science (JSPS), and the Collaborative Research Projects of Laboratory for Materials and Structures, Institute of Innovative Research, Tokyo Institute of Technology. The SXRD experiments were performed under the approval of the Photon Factory Program Advisory Committee (Proposal No. 2019G566).

[1] C. Broholm, R. J. Cava, S. A. Kivelson, D. G. Nocera, M. R. Norman, and T. Senthil, Quantum spin liquids, Science **367**, eaay0668 (2020).

[2] S. E. Sebastian, N. Harrison, C. D. Batista, L. Balicas, M. Jaime, P. A. Sharma, N. Kawashima, and I. R. Fisher, Dimensional reduction at a quantum critical point, Nature (London) **441**, 617 (2006).

[3] O. A. Starykh, Unusual ordered phases of highly frustrated magnets: a review, Rep. Prog. Phys. **78**, 052502 (2015).

[4] I. Affleck, Quantum spin chains and the haldane gap, J. Phys.: Condens. Matter **1**, 3047 (1989).

[5] E. Dagotto and T. M. Rice, Surprises on the way from one- to two-dimensional quantum magnets: The ladder materials, Science **271**, 618 (1996).

[6] M. Goto, H. Ueda, C. Michioka, A. Matsuo, K. Kindo, and K. Yoshimura, Various disordered ground states and $\frac{1}{3}$ magnetization-plateau-like behavior in the $s = \frac{1}{2}$ Ti^{3+} kagome lattice antiferromagnets $Rb_2NaTi_3F_{12}$, $Cs_2NaTi_3F_{12}$, and $Cs_2KTi_3F_{12}$, Phys. Rev. B **94**, 104432 (2016).

[7] L. Clark, J. C. Orain, F. Bert, M. A. De Vries, F. H. Aidoudi, R. E. Morris, P. Lightfoot, J. S. Lord, M. T. F. Telling, P. Bonville, J. P. Attfield, P. Mendels, and A. Harrison, Gapless Spin Liquid Ground State in the $S = 1/2$ Vanadium Oxyfluoride Kagome Antiferromagnet $[NH_4]_2[C_7H_{14}N][V_7O_6F_{18}]$, Phys. Rev. Lett. **110**, 207208 (2013).

[8] J. R. Chamorro, T. M. McQueen, and T. T. Tran, Chemistry of quantum spin liquids, Chem. Rev. (Washington, DC) **121**, 2898 (2021).

[9] D. Inosov, Quantum magnetism in minerals, Adv. Phys. **67**, 149 (2019).

[10] P. Khuntia, M. Velazquez, Q. Barthélemy, F. Bert, E. Kermarrec, A. Legros, B. Bernu, L. Messio, A. Zorko, and P. Mendels, Gapless ground state in the archetypal quantum kagome antiferromagnet $ZnCu_3(OH)_6Cl_2$, Nat. Phys. **16**, 469 (2020).

[11] R. W. Smaha, W. He, J. M. Jiang, J. Wen, Y.-F. Jiang, J. P. Sheckelton, C. J. Titus, S. G. Wang, Y.-S. Chen, S. J. Teat, A. A. Aczel, Y. Zhao, G. Xu, J. W. Lynn, H.-C. Jiang, and Y. S. Lee, Materializing rival ground states in the barlowite family of kagome magnets: quantum spin liquid, spin ordered, and valence bond crystal states, npj Quantum Mater. **5**, 23 (2020); **5**, 24(E) (2020); **5**, 48(E) (2020).

[12] H. Kikuchi, Y. Fujii, M. Chiba, S. Mitsudo, T. Idehara, T. Tonegawa, K. Okamoto, T. Sakai, T. Kuwai, and H. Ohta, Experimental Observation of the 1/3 Magnetization Plateau in the Diamond-Chain Compound $Cu_3(CO_3)_2OH_2$, Phys. Rev. Lett. **94**, 227201 (2005).

[13] H. Jeschke, I. Opahle, H. Kandpal, R. Valentí, H. Das, T. Saha-Dasgupta, O. Janson, H. Rosner, A. Brühl, B. Wolf, M. Lang, J. Richter, S. Hu, X. Wang, R. Peters, T. Pruschke, and A. Honecker, Multistep Approach to Microscopic Models for Frustrated Quantum Magnets: The Case of the Natural Mineral Azurite, Phys. Rev. Lett. **106**, 217201 (2011).

[14] M. Fujihala, K. Morita, R. Mole, S. Mitsuda, T. Tohyama, S.-i. Yano, D. Yu, S. Sota, T. Kuwai, A. Koda, H. Okabe, H. Lee, S. Itoh, T. Hawai, T. Masuda, H. Sagayama, A. Matsuo, K. Kindo, S. Ohira-Kawamura, and K. Nakajima, Gapless spin liquid in a square-kagome lattice antiferromagnet, Nat. Commun. **11**, 3429 (2020).

[15] I. Nakai, H. Okada, K. Masutomi, E. Koyama, and K. Nagashima, Henmilite, $Ca_2Cu(OH)_4[B(OH)_4]_2$, a new mineral from Fuka, Okayama Prefecture, Japan; I, Occurrence and description, Am. Mineral. **71**, 1234 (1986).

[16] I. Nakai, H. Okada, K. Masutomi, E. Koyama, and K. Nagashima, Henmilite, $Ca_2Cu(OH)_4[B(OH)_4]_2$, a new mineral from Fuka, Okayama Prefecture, Japan; II, Crystal structure, Am. Mineral. **71**, 1236 (1986).

[17] K. Foyevtsova, I. Opahle, Y.-Z. Zhang, H. O. Jeschke, and R. Valentí, Determination of effective microscopic models for the frustrated antiferromagnets Cs_2CuCl_4 and Cs_2CuBr_4 by density functional methods, Phys. Rev. B **83**, 125126 (2011).

[18] E. Ruiz, P. Alemany, S. Alvarez, and J. Cano, Structural modeling and magneto-structural correlations for hydroxo-bridged copper(II) binuclear complexes, Inorg. Chem. **36**, 3683 (1997).

[19] S. Lebernegg, A. A. Tsirlin, O. Janson, and H. Rosner, Two energy scales of spin dimers in clinoclase $Cu_3(AsO_4)(OH)_3$, Phys. Rev. B **87**, 235117 (2013).

[20] Y. Iqbal, H. O. Jeschke, J. Reuther, R. Valentí, I. I. Mazin, M. Greiter, and R. Thomale, Paramagnetism in the kagome compounds $(Zn, Mg, Cd)Cu_3(OH)_6Cl_2$, Phys. Rev. B **92**, 220404(R) (2015).

[21] M. Azuma, Z. Hiroi, M. Takano, K. Ishida, and Y. Kitaoka, Observation of a Spin Gap in $SrCu_2O_3$ Comprising Spin-$^1/_2$ Quasi-1D Two-Leg Ladders, Phys. Rev. Lett. **73**, 3463 (1994).

[22] S. Gopalan, T. M. Rice, and M. Sigrist, Spin ladders with spin gaps: A description of a class of cuprates, Phys. Rev. B **49**, 8901 (1994).

[23] T. Rice, S. Gopalan, and M. Sigrist, Superconductivity, spin gaps and Luttinger liquids in a class of cuprates, Europhys. Lett. **23**, 445 (1993).

[24] M. Sigrist, T. M. Rice, and F. C. Zhang, Superconductivity in a quasi-one-dimensional spin liquid, Phys. Rev. B **49**, 12058 (1994).

[25] Y. Satow and Y. Iitaka, Horizontal-type four-circle diffractometer station of the vertical wiggler beamline at the photon factory, Rev. Sci. Instrum. **60**, 2390 (1989).

[26] K. Tanaka, S. Kumazawa, M. Tsubokawa, S. Maruno, and I. Shirotani, The multiple-diffraction effect in accurate structure-factor measurements of PtP_2 crystals, Acta Crystallogr. A: Found. Crystallogr. **50**, 246 (1994).

[27] S. Kishimoto, N. Ishizawa, and T. P. Vaalsta, A fast detector using stacked avalanche photodiodes for x-ray diffraction experiments with synchrotron radiation, Rev. Sci. Instrum. **69**, 384 (1998).

[28] S. Kishimoto, Avalanche photodiodes as fast X-ray detectors, J. Synchroton Radiat. **5**, 275 (1998).

[29] See Supplemental Material at http://link.aps.org/supplemental/10.1103/PhysRevMaterials.5.104405 for further details.

[30] K. Momma and F. Izumi, *VESTA3* for three-dimensional visualization of crystal, volumetric and morphology data, J. Appl. Crystallogr. **44**, 1272 (2011).

[31] K. Koepernik and H. Eschrig, Full-potential nonorthogonal local-orbital minimum-basis band-structure scheme, Phys. Rev. B **59**, 1743 (1999).

[32] J. P. Perdew, K. Burke, and M. Ernzerhof, Generalized Gradient Approximation Made Simple, Phys. Rev. Lett. **77**, 3865 (1996).

[33] A. I. Liechtenstein, V. I. Anisimov, and J. Zaanen, Density-functional theory and strong interactions: Orbital ordering in Mott-Hubbard insulators, Phys. Rev. B **52**, R5467(R) (1995).

[34] H. O. Jeschke, F. Salvat-Pujol, and R. Valentí, First-principles determination of Heisenberg Hamiltonian parameters for the spin-$\frac{1}{2}$ kagome antiferromagnet $ZnCu_3(OH)_6Cl_2$, Phys. Rev. B **88**, 075106 (2013).

[35] D. Guterding, R. Valentí, and H. O. Jeschke, Reduction of magnetic interlayer coupling in barlowite through isoelectronic substitution, Phys. Rev. B **94**, 125136 (2016).

[36] R. Kiyanagi, A. Kojima, H. Kimura, M. Watanabe, Y. Noda, T. Mochida, and T. Sugawara, Phase transition scheme of isolated hydrogen-bonded material h-MeHPLN studied by neutron and X-ray diffraction, J. Phys. Soc. Jpn. **74**, 613 (2005).

[37] R. Kiyanagi, H. Kimura, M. Watanabe, Y. Noda, T. Mochida, and T. Sugawara, Indication of tunneling state of hydrogen atom in hydrogen-bonded material 5-bromo-9-hydroxyphenalenon studied by X-ray and neutron diffractions, J. Phys. Soc. Jpn. **77**, 064602 (2008).

[38] D. C. Johnston, Normal-state magnetic properties of single-layer cuprate high-temperature superconductors and related materials, in *Handbook of Magnetic Materials* (Elsevier, New York, 1997), Vol. 10, Chap. 1, pp. 1–237.

[39] K. Oka, I. Yamada, M. Azuma, S. Takeshita, K. H. Satoh, A. Koda, R. Kadono, M. Takano, and Y. Shimakawa, Magnetic ground-state of perovskite $PbVO_3$ with large tetragonal distortion, Inorg. Chem. **47**, 7355 (2008).

[40] S. Nakatsuji, Y. Nambu, H. Tonomura, O. Sakai, S. Jonas, C. Broholm, H. Tsunetsugu, Y. Qiu, and Y. Maeno, Spin disorder on a triangular lattice, Science **309**, 1697 (2005).

[41] D. P. Landau and K. Binder, Phase diagrams and critical behavior of a two-dimensional anisotropic Heisenberg antiferromagnet, Phys. Rev. B **24**, 1391 (1981).

[42] A. A. Tsirlin, O. Janson, S. Lebernegg, and H. Rosner, Square-lattice magnetism of diaboleite $Pb_2Cu(OH)_4Cl_2$, Phys. Rev. B **87**, 064404 (2013).

[43] R. Nath, A. A. Tsirlin, H. Rosner, and C. Geibel, Magnetic properties of $BaCdVO(PO_4)_2$: A strongly frustrated spin-$\frac{1}{2}$ square lattice close to the quantum critical regime, Phys. Rev. B **78**, 064422 (2008).

[44] P. Sengupta, C. D. Batista, R. D. McDonald, S. Cox, J. Singleton, L. Huang, T. P. Papageorgiou, O. Ignatchik, T. Herrmannsdörfer, J. L. Manson, J. A. Schlueter, K. A. Funk, and J. Wosnitza, Nonmonotonic field dependence of the Néel temperature in the quasi-two-dimensional magnet $[Cu(HF_2)(pyz)_2]BF_4$, Phys. Rev. B **79**, 060409(R) (2009).

[45] Y. Iqbal, T. Müller, K. Riedl, J. Reuther, S. Rachel, R. Valentí, M. J. P. Gingras, R. Thomale, and H. O. Jeschke, Signatures of a gearwheel quantum spin liquid in a spin-$\frac{1}{2}$ pyrochlore molybdate Heisenberg antiferromagnet, Phys. Rev. Mater. **1**, 071201(R) (2017).

[46] L. Heinze, H. O. Jeschke, I. I. Mazin, A. Metavitsiadis, M. Reehuis, R. Feyerherm, J.-U. Hoffmann, M. Bartkowiak, O. Prokhnenko, A. U. B. Wolter, X. Ding, V. S. Zapf, C. Corvalán Moya, F. Weickert, M. Jaime, K. C. Rule, D. Menzel, R. Valentí, W. Brenig, and S. Süllow, Magnetization Process of Atacamite: A Case of Weakly Coupled $S = 1/2$ Sawtooth Chains, Phys. Rev. Lett. **126**, 207201 (2021).

[47] K. Iida, H. K. Yoshida, A. Nakao, H. O. Jeschke, Y. Iqbal, K. Nakajima, S. Ohira-Kawamura, K. Munakata, Y. Inamura, N. Murai, M. Ishikado, R. Kumai, T. Okada, M. Oda, K. Kakurai, and M. Matsuda, $q = 0$ long-range magnetic order in centennialite $CaCu_3(OD)_6Cl_2 \cdot 0.6D_2O$: A spin-$\frac{1}{2}$ perfect kagome antiferromagnet with $J_1 - J_2 - J_d$, Phys. Rev. B **101**, 220408(R) (2020).

[48] S. Chillal, Y. Iqbal, H. O. Jeschke, J. A. Rodriguez-Rivera, R. Bewley, P. Manuel, D. Khalyavin, P. Steffens, R. Thomale, A. T. M. N. Islam, J. Reuther, and B. Lake, Evidence for a three-dimensional quantum spin liquid in $PbCuTe_2O_6$, Nat. Commun. **11**, 2348 (2020).

[49] C. Yasuda, S. Todo, F. Hukushima, K. Alet, M. Keller, M. Troyer, and H. Takayama, Néel Temperature of Quasi-Low-Dimensional Heisenberg Antiferromagnets, Phys. Rev. Lett. **94**, 217201 (2005).

[50] M. Matsumoto, C. Yasuda, S. Todo, and H. Takayama, Ground-state phase diagram of quantum Heisenberg antiferromagnets on the anisotropic dimerized square lattice, Phys. Rev. B **65**, 014407 (2001).